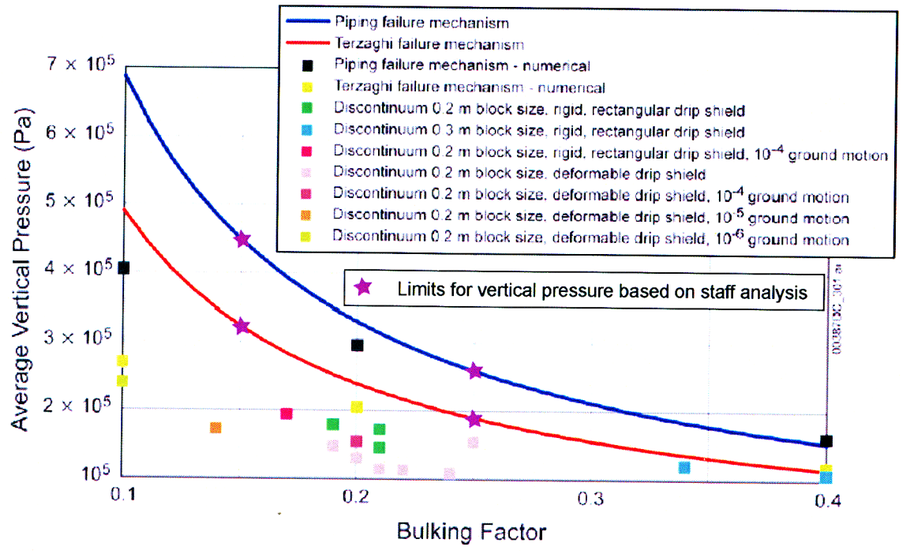

Figure 14 Vertical Load on the Drips Shield as a Function of the Bulking Factor (from DOE, Drift Degradation Analysis)

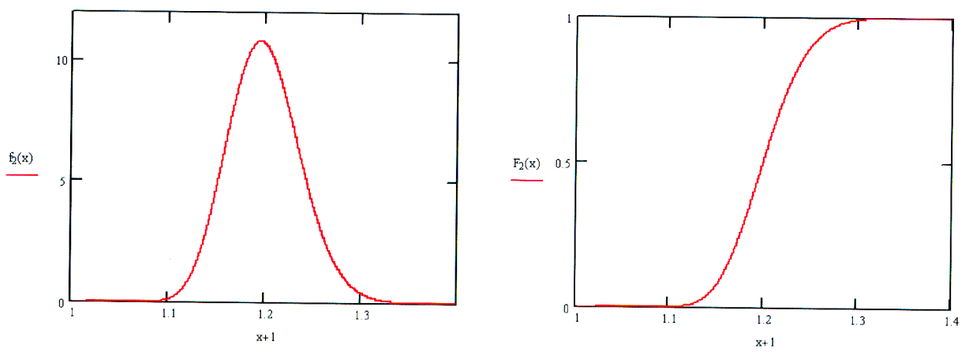

Figure 15 PDF and CDF for Bulking Factor

03-07-06

Drift Degradation Time (Demands)

In addition to the magnitude of the average vertical pressure, the drift degradation time has to be estimated. The current abstraction in the TPA code is based on the beta distribution proposed in MECHFAIL 2003, in which all drifts fail during the first 1000 years. For the updated abstractions an unbounded lognormal is proposed to recognize that some drift sections may remain in place for periods larger than 1000 years. The proposed lognormal distribution has a median value of 750 years and a standard deviation of the log of the data of 0.23 (**Figure 16**), resulting in the following probabilities for different intervals:

P[t < 400 years] = 0.31 %
P[t < 500 years] = 3.90 %
P[t < 1,000 years] = 89.45 %
P[t < 1280 years] = 99.00 %

03-07-06

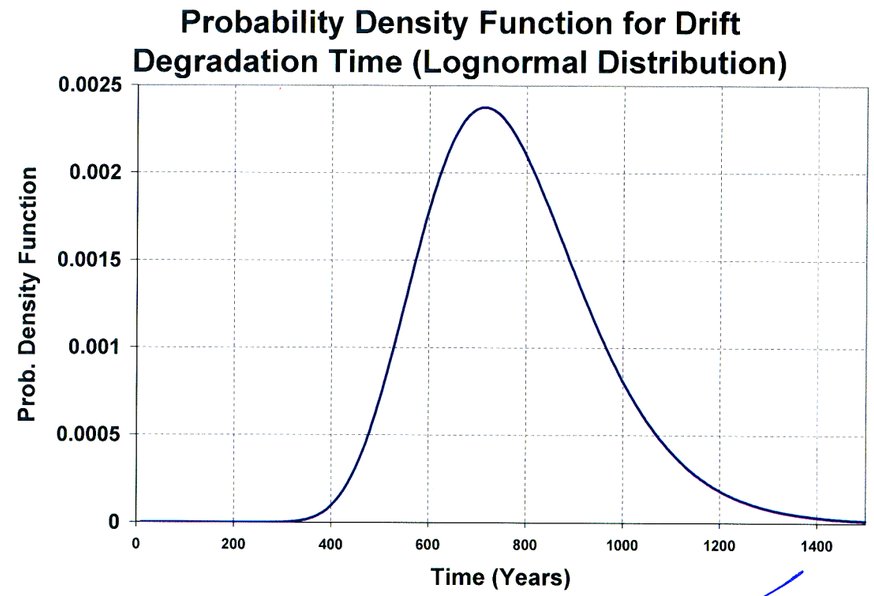

Figure 16a

03-07-06

DS Vertical Load Carrying Capacity

In addition to the average vertical pressure, the DS vertical load carrying capacity is affected by several additional parameters, such as the static loading configuration, temperature, etc. The abstractions for the DS capacity are based on the static loading configuration, which is defined by the horizontal to vertical load ratio and lateral load imbalance. However, the horizontal to vertical load ratio is the only parameter included in the abstraction because the imbalance load has a much smaller effect on the DS vertical load carrying capacity, an effect that decreases as the rubble column increases. After the DS vertical load carrying capacity is estimated based on the horizontal to vertical load ratio, it is corrected by other factors such as temperature and creeping.

According to the discussion of Appendix A, the median value for the horizontal to vertical load ratio is proposed at P_h/P_v = 0.5, the lower limit slightly smaller than P_h/P_v = 0.20, and the upper limit at P_h/P_v = 1.0. Based on this information, a standard beta distribution is selected with mean = 0.5, and standard deviation = 0.11. The distribution is presented in **Figure 17a**, and the probabilities for several intervals are presented below:

$P[P_h/P_v < 0.20] = 0.17$ %
$P[P_h/P_v < 0.50] = 50.0$%
$P[P_h/P_v < 0.80] = 99.8$ %
$P[P_h/P_v < 1.00] = 100.0$ %

Once the horizontal to vertical load ratio is selected, the variation of the DS vertical load carrying capacity to this parameter can be estimated by the equations fitted to the results obtained from the DS structural report. **Figure 17b** presents this fitting.

Temperature (DS)

The effect of temperature on DS capacity is included by introducing a multiplier that affects the vertical load carrying capacity. After the drift degrades, the temperature increase and the DS capacity is adjusted accordingly. The following temperature factors are obtained from the DS structural performance report:

F_{temp} = 1.0 for $T \leq$ 150 degrees Celsius
F_{temp} = 0.78 for T = 260 degrees Celsius
F_{temp} = 0.64 for $T \geq$ 316 degrees Celsius

For intermediate temperatures, the temperature factor is linearly interpolated. Staff is considering whether to evaluate the DS capacity for temperatures lower than 150 C. Under this scenario, there could be multiplier factors larger than one for temperatures lower than 150 C. On the other hand, the highest temperature T = 316 C may occur when the drift degrades almost immediately after closure of the repository.

The DS vertical load carrying capacity obtained from the DS capacity abstraction is corrected by the temperature factor as follows,

$$P_{v,cap} = P_{v,cap} * F_{temp}$$

03-07-06

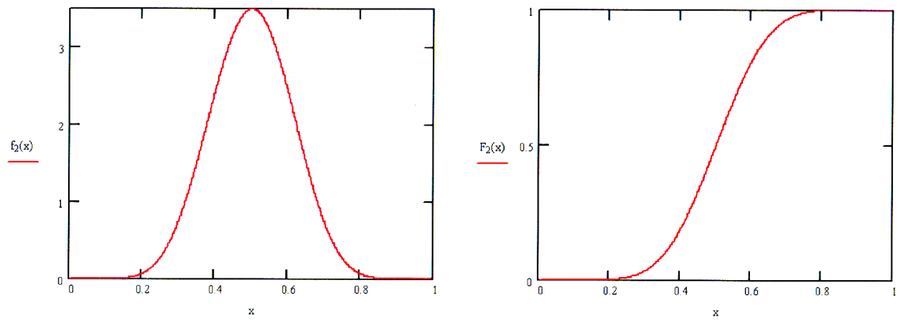

Figure 17a

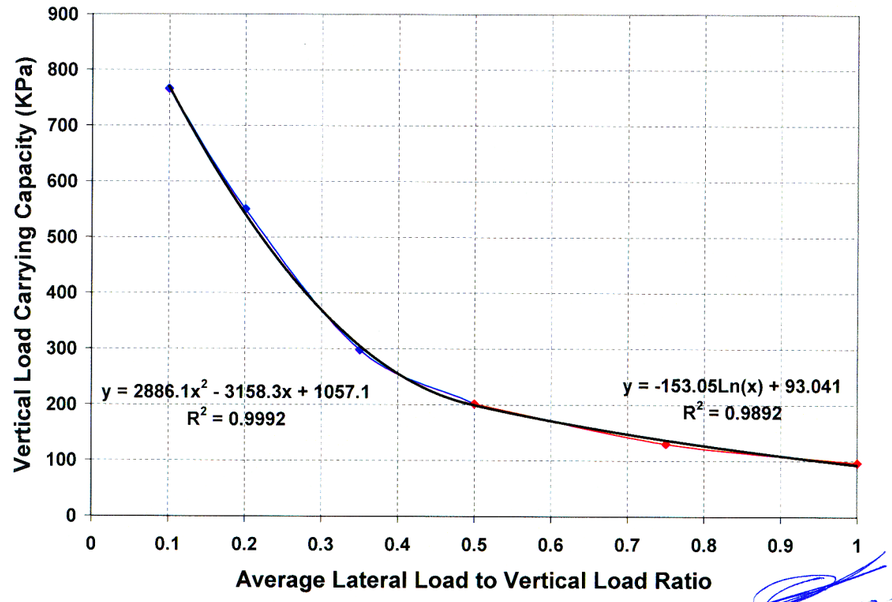

Figure 17b

03-07-06

The fitted curve of Fig. 17b was changed to a polynomial one to be incorporated into the TPA code.

Creeping (D3)

03-07-06

Creeping of titanium materials depend on several factors such as the stress level of the component, temperature, and micro-structure of the material. Although temperature modifies creeping performance, most experiments have been performed at room temperature. Thus, there is no systematic information about the effect of temperature on creeping of titanium materials. For Ti-5 (surrogate material for Ti-24), the type of micro-structure modifies the stress level at which creeping initiates. Results from a literature survey on the topic indicate that creeping of Ti-5 may start for stress levels as low as 25% of the yield stress, $\sigma = 0.25\sigma_y$, and as high as $\sigma = 0.80\sigma_y$. Nevertheless, creeping may lead to strains associated to the ultimate tensile strength of the material only when the stress levels are close to the yield stress, $\sigma > 0.90\sigma_y$. Furthermore, if the yield stress is not reached, creeping effects would lead to strains associated to the ultimate tensile strength after several thousands of years. But if the structural system exceeds the yield stresses, the creeping effects will be largely accelerated.

For the TPA code, creeping effects will be included once the yield stresses are surpassed. Because of the lack of information, at this stage will be assumed a uniform distribution for the creeping threshold with lower boundary of $\sigma = \sigma_y$, and an upper boundary associated to the structural instability of the material. According to the DS report (2005), the DS baseline model starts to exhibit nonlinear behavior for vertical pressures P_v = 188 Kpa. That is to say, at about 63% of the ultimate failure of the DS system. Then, the DS capacity is estimated after randomly obtaining the creeping onset from a uniform distribution between 63% (approximately the inelastic behavior threshold) and 100% of the ultimate load carrying capacity.

$$P_{v,cap} = P_{v,cap} * F_{creep}$$

where F_{creep} is randomly selected based on a uniform distribution.

All the above information about creeping has to be corroborated once the report on literature survey on creeping is complete.

Generalized Corrosion (D3)

03-07-06

According to the DOE (TBD-14), the effect of generalized corrosion on the DS causes a reduction of 2 mm on the thickness of the titanium plates for the first 10,000 years, which was the original postclosure regulatory period. As presented in the DS report (DS 2005), the vertical load carrying capacity decreases approximately 10% due to this 2 mm-thinning of the plates. The degradation of the drift, however, will very likely take place during the first 1,000 years after closure of the repository. During the first 1,000 years, the thinning of the plates due to generalized corrosion will be much smaller than the DOE proposal of 2 mm. Therefore, the effect on the vertical load carrying capacity of the DS under permanent vertical load will be negligible.

The effect of generalized corrosion could have been relevant when evaluating the capacity of the DS under dynamic loading, which may happen at any time during the regulatory period. However, the DS report shows that a DS supporting static loading due to rockfall cannot withstand seismic ground motions associated to MAPEs of 10-5 or smaller. Therefore, the thinning of the plates for the seismic analyses is not required.

Invert Degradation

The invert of the drift is composed of a grid of carbon-steel beams and tuff material. Initially, the DS rests on the grid of carbon-steel beams, however, the beams are likely to corrode relatively fast. If the degradation rate of the beams is not uniform, the DS may experience significant differential settlements, particularly because the bearing capacity of the tuff soil may be largely exceeded under the loads transferred by the DS. Differential settlements of the DS may decrease further the vertical load carrying capacity. Because of the available limited information, however, the proposed abstractions do not include this potential failure mechanism. It is anticipated that this omission will not affect the overall DS performance because most of the DSs should reach collapse.

03-07-06

March 10, 2006

ABSTRACTIONS WP

The initial static loading for the DS-WP interaction is the same load applied to the DS at the onset of DS structural instability. After some time, the loading may be slightly larger because the DS collapse will create a void that eventually should be filled. Also, the rubble will compact with time and after each seismic event. The soil compaction affects both the subsequent permanent static loading and inertial forces of subsequent seismic events. However, compaction is not relevant for subsequent permanent static loading because these loads are bounded by the dynamic loads that lead to soil compaction (i.e., if the WP was able to withstand the dynamic amplifications, it should be able to resist the increase in permanent static loading). On the other hand, subsequent seismic events are affected because the inertial forces will be larger when including a larger permanent static load.

03-10-06

Static Loading

Contact Angle, α

03-10-06

The contact angle varies according to several parameters. The bulkhead and the longitudinal stiffeners are the DS components with sharp edges that may rest on the WP OS with a certain contact angle. The sources for this contact angle have been described above. Nevertheless, it is expected that this parameter will be relatively small, with values smaller than 10 degrees. However, sometimes the collapse of the DS will be partial or very localized. In these situations, the contact angle may be much larger than 10 degrees. The Cauchy distribution of **Figure 18** includes a large percentage of its area (85%) in the [-10, 10] degree interval. The distribution is

similar to a normal one, but has heavier tails to account for situations in which the contact angle may be much larger than 10 degrees. This Cauchy distribution was favored over the normal distribution because is not possible to capture a large part of the realizations around the [-10, 10] degree interval, and still obtain realizations with contact angles close to 45 degrees. For instance, a normal distribution requires a standard deviation of 7.5 in order to have a probability of 85% of having the contact angle within the [-10, 10] degree interval. Therefore, contact angles with standard deviations larger than 22.5 (about 3 standard deviations) have a probability of occurrence of less than 0.1%.

The general formula for the probability density function of the Cauchy distribution is,

$$f_X(x) = \frac{1}{\pi}\frac{s}{(x-L)^2 + s^2}$$

where L is the location parameter and s is the scale parameter. For the contact angle, the Cauchy distribution range is [-45,45], the median = L = 0, and s = 2.4. Based on these parameters, the following probabilities of occurrence for different intervals are obtained from the CDF:

P[α < -40] = 1.9 %
P[α < -30] = 2.5 %
P[α < - 10] = 7.5%
P[α < 10] = 92.5%
P[-10 < α < 10] = 85%

03-10-06

CAUCHY DIST.

PDF = $\frac{1}{\pi}\cdot\frac{S}{(x-L)^2 + S^2}$

03-10-06

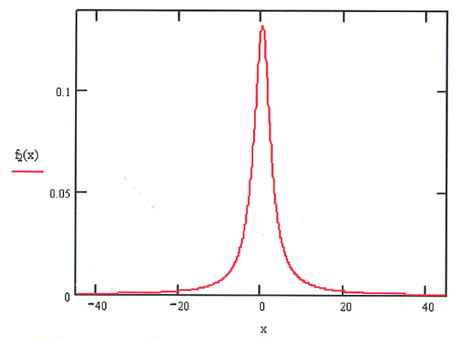

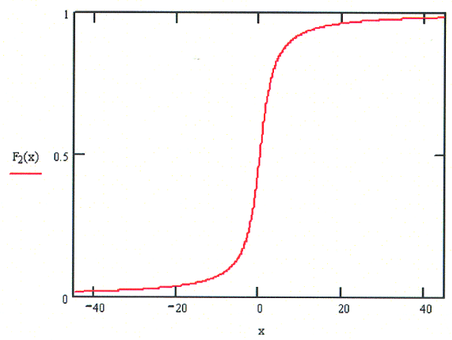

The above Cauchy distribution was changed by a lognormal distribution with mean = 0 and σ = 10, because although the Cauchy dist. was able to capture relatively large angles, it was probably overestimating the realizations with very

small contact angles. The new distribution is shown below:

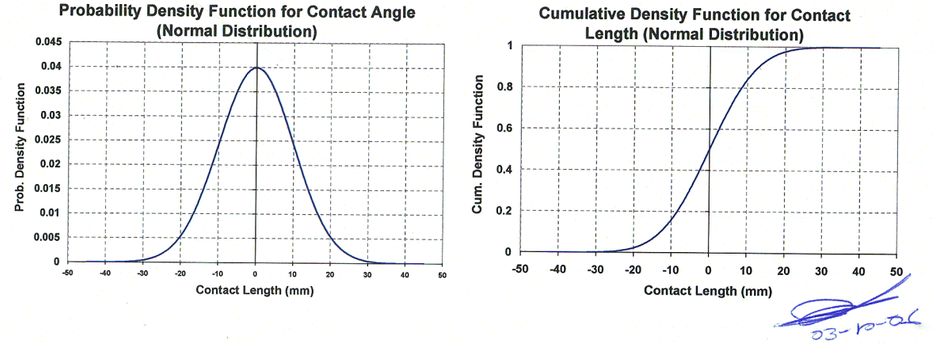

03-10-06

Once the contact angle is known, the force per unit length can be obtained according to the sensitivity study performed for the plane strain model. See figure below:

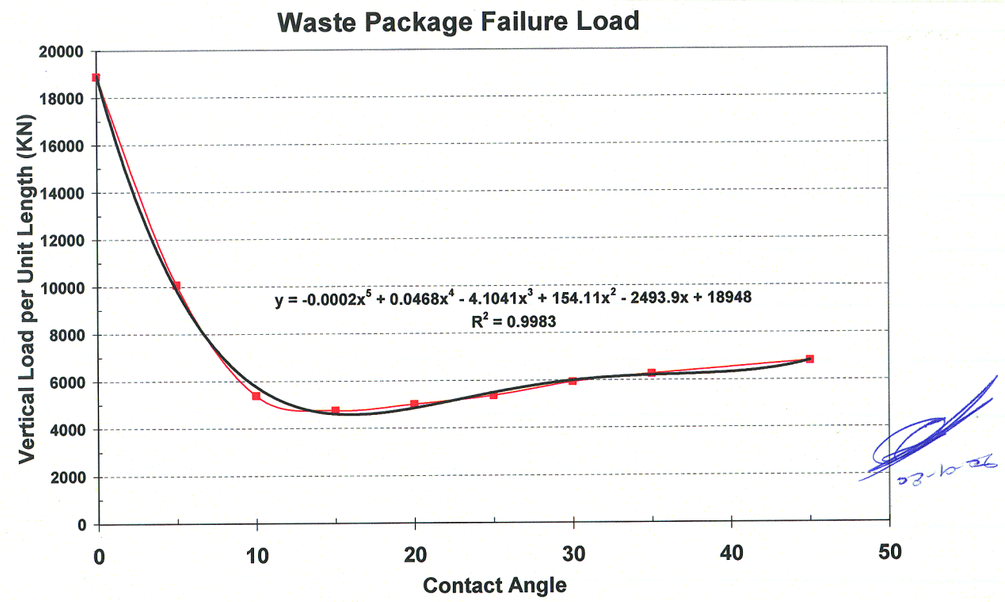

03-10-06

This figure, however, is based on a permissible strain $\varepsilon_{B,live} = 0.33$ (see page 63). When stress-strain curves were obtained from

tensile tests, the strain at UTS was at least $\varepsilon_{Failure} = 0.75$. Then, new analyses were performed for the new data.

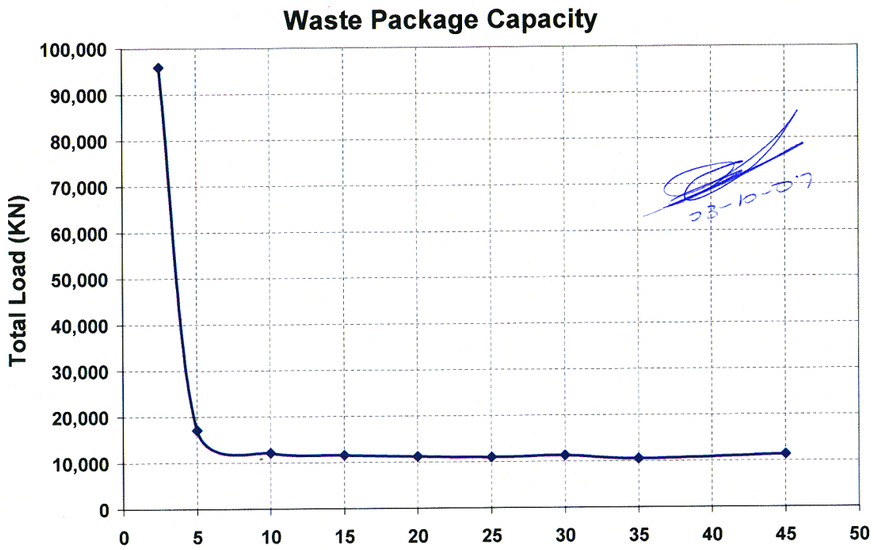

Contact Angle

the WP capacity doubled when the new double strains were introduced.

Contact Length

According to the data obtained from the 3-D FEMs in ABAQUS, the contact length between the DS component and the WP OS is a parameter that tends to increase as the load level increases. The parameter is used to obtain an equivalent pressure from the plane strain model. For the MECHFAIL abstraction, the contact length is obtained from a proposed normal distribution with mean value of 500 mm and standard deviation of 100 mm, **Figure 20**. The expected values on potential variations are obtained from the 3-D FEM results. Once the TPA code selects a random value for this parameter, the WP OS capacity can be expressed in terms of vertical pressure.

23-10-07

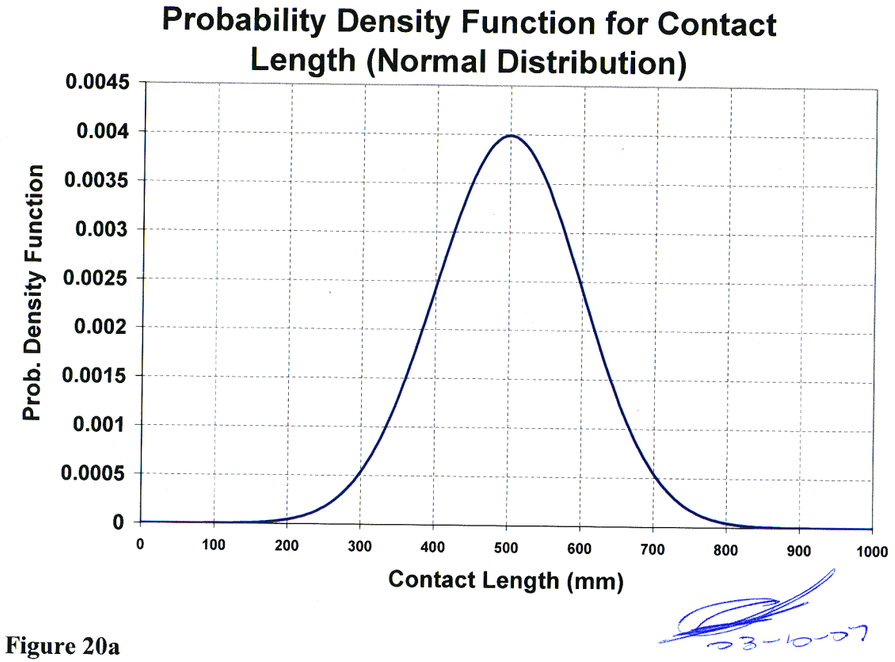

Figure 20a

Tangential Loads

As observed in **Figures 10c and 10d**, tangential forces may increase the OS capacity when subjected to static loads transferred by the DS, because the contact area increases under this loading configuration. This increase in the WP capacity is not included in the abstractions for several reasons. First, the tangential forces are not evenly distributed as the DS wraps around the WP OS because of variations in the angle between the gravity load and the tangent to the OS surface. Second, under relatively symmetrical DS collapse, the initial contact region will be at the top of the WP, where the load is applied perpendicular to the tangent of the OS. Third, the tangential loads improve the WP capacity mainly at places where the bulkhead cross section does not include the longitudinal stiffener. As shown above, the bulkhead bottom flange predicts early WP failure likely due to the development of local shear stresses. Therefore, the tangential forces will not be included in the abstractions until better FEMs predict are implemented.

23-10-07

Alloy-22 Plate Thickness

The thickness of the Alloy-22 plate may decrease after several hundred thousand years due to generalized corrosion. The potential for breaching of the WP OS will increase as the plate thickness is reduced even if the inner vessel is considered a rigid surface because of the modification of the displacement field. **Figure 21** presents the power equation that is used to fit a curve to the variation of the WP OS capacity for different plate thicknesses. The results correspond to a model with a contact angle of 15 degrees. The multiplier resulting from this equation will be used at different angles. Then, the force or vertical load carrying capacity of the WP OS reduces as the thickness plate reduces, according to the following equation,

$$P_{v,cap} = P_{v,cap} F_{tp}$$

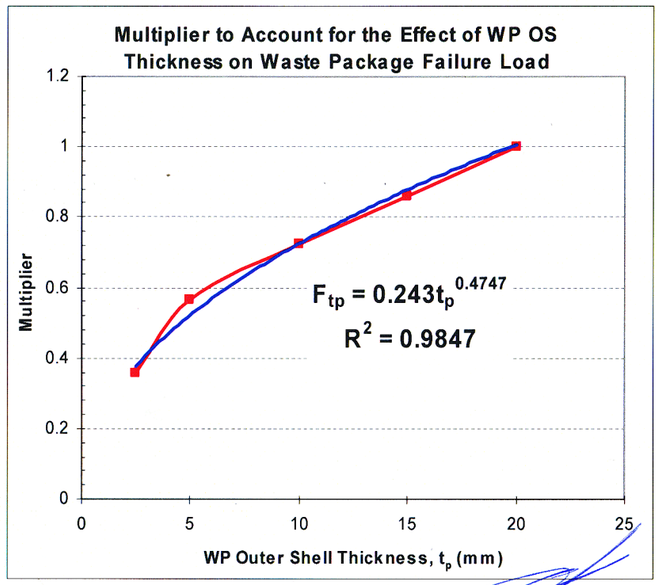

Figure 21

Dynamic Loading

Seismic Ground Motions

Most DSs collapse under static loading, however, DS-WP mechanical interaction usually does not result in breaching of the WP OS, and the loads transferred to the WP may be amplified due to seismic ground motions. The abstraction at this stage for the dynamic loading will be an approximation based on the increase of the permanent vertical loads due to the peak ground acceleration during a seismic event. This rather simplistic approach does not permit the evaluation of cumulative damage because the seismic effect is approximated based on a comparison of demand versus allowable loads, without including permanent deformation of the WP. Nevertheless, some effects due to multiple seismic events are accounted for in the TPA code. For instance, the permanent vertical pressure increases after each seismic event because the soil consolidates. Also, because the PGV is the earthquake intensity measure, different seismic events have different PGAs. Then, different seismic events with exactly the same MAPE may result in different outcome because the PGA is a random variable for the same PGV value.

The seismic hazard is derived from ground motion records developed by DOE, which are deemed to be adequate for the repository level. The seismic scenario has been discretized in several earthquake levels associated with mean annual probability of exceedance (MAPE) of $1x10^{-4}$, $1x10^{-5}$, $1x10^{-6}$, and $1x10^{-7}$. For each earthquake level, sets of velocity and acceleration time histories, as well as site response spectra for the waste emplacement level are available.

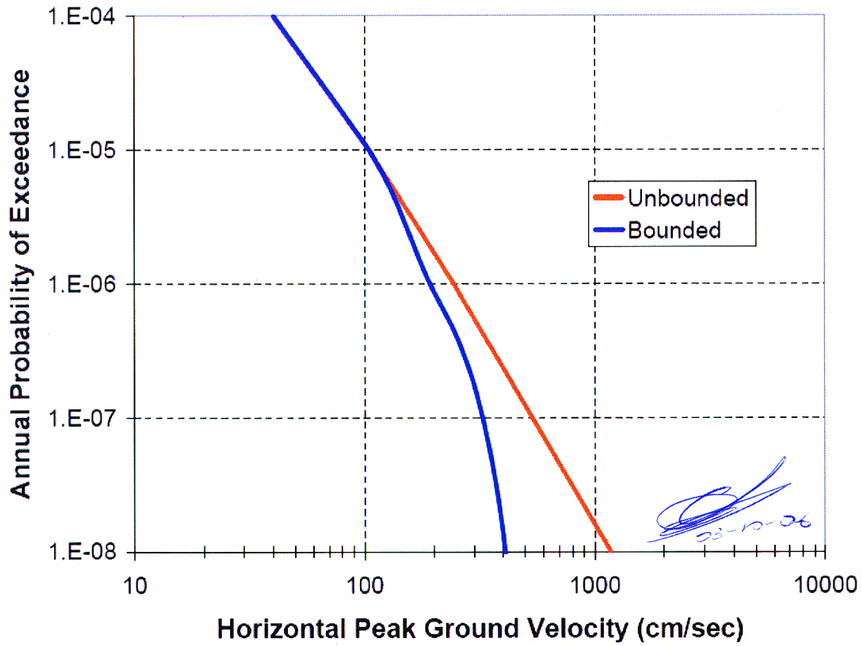

Figure 22

In addition, site values for the expected (target) peak ground velocity (PGV) were computed for some of the above seismic levels, see **Table 1**. These PGV magnitudes are used to scale time histories and to develop a ground motion hazard curve for the waste emplacement level. The hazard curve is based on the PGV parameter, which is the intensity measure of the earthquake level for this study.

Table 1. Site Peak Ground Velocity for the Waste Emplacement Level	
MAPE	Horizontal PGV (m/s)
10^{-5}	1.05
10^{-6}	2.44
10^{-7}	5.35

The information presented in **Table 1** is also included in the unbounded seismic hazard curve proposed by DOE (see **Figure 22**). The DOE has recently suggested the use of a bounded hazard curve with a PGV capped at 4 m/s. Because this curve is still under review, the TPA code will include the unbounded hazard curve, with the difference that PGVs will be arbitrarily capped at 5.35 m/s. That is to say, any seismic event with a MAPE lower than 10^{-7} will have a PGV value of 5.35 m/s. The statistical TPA results are not significantly affected by this capping value because of the very low likelihood of these events.

For the ground motions associated with MAPEs of 10^{-5}, 10^{-6} and 10^{-7}, the DOE has proposed a subset of 15 records that includes 12 Californian records. The original records are scaled to a target horizontal PGV based on the MAPE (**Table 1**). To preserve intercomponent variability, the other two orthogonal directions are scaled in the same proportion, which sometimes causes the target PGV to be exceeded in the other two directions. The magnitude of PGA is also controlled by the scaling factor of the PGV. Because ATHs are obtained from integrating the VTH, even the PGA data in the direction of the original scaling exhibits dispersion. For instance, **Figure 23** shows the individual PGV and PGA values, as well as the mean, 16th, 50th, and 84th fractiles. As discussed, the PGA values show dispersion in the three orthogonal directions because the scaling depends on the PGV.

The largest MAPE considered for seismic events will be $1x10^{-4}$. It is unlikely that the WP OS withstanding static loading will fail under a seismic event associated to a MAPE of 10^{-4}. Nevertheless, PGA variability may occasionally result in large accelerations for seismic events with MAPEs between 10^{-5} and 10^{-4}. Also, compaction of the rubble surrounding the DS occurs for seismic events with moderate to large accelerations. Thus, the analyses considers that compaction of the rubble cannot be neglected after seismic events with MAPEs of $1x10^{-4}$ or lower. An effect that will result in the static vertical pressure to be amplified in subsequent earthquakes. Finally, seismic events with MAPE of 10^{-4} may accelerate drift degradation if they occur previous to complete natural degradation.

Poisson Distribution

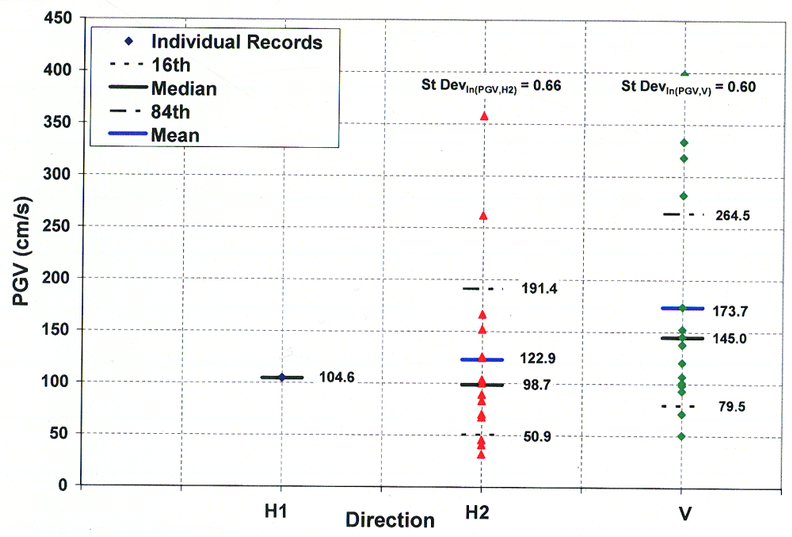

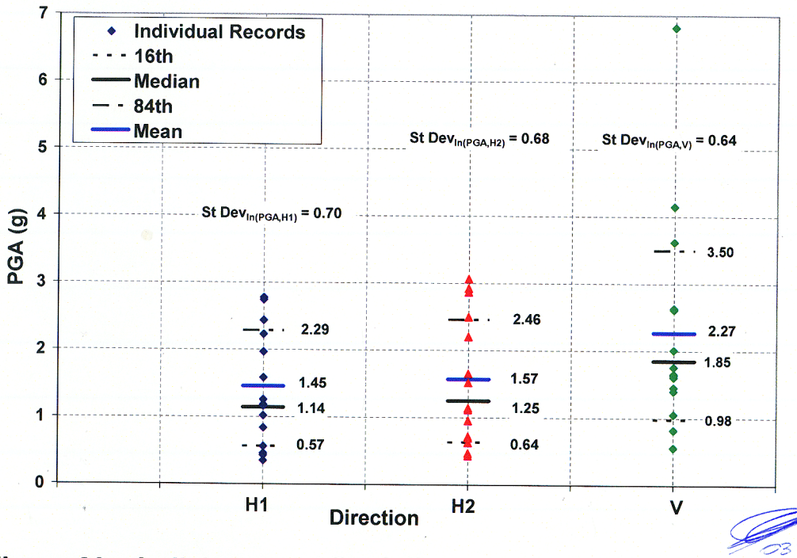

Figure 23 Individual and Statistical PGV and PGA Data for the Subset of 15 Ground Motions, MAFE of 10^{-5}, a) PGV, b) PGA

A Poisson distribution is assumed for the occurrence of seismic events:

$$P_N(n) = \frac{\lambda^n e^{-\lambda}}{n!} \qquad (1)$$

where λ is the probability of occurrence of the seismic event, and can be expressed as $\lambda = \nu t$, where ν is the mean rate of occurrence of the event (i.e., MAPE), and t is the time in which the event can take place. The mean rate of occurrence is the reciprocal of the return period, $\nu = 1/T$. **Table 2** presents the number of seismic events expected for 10,000 years for different MAPEs.

Multiple Seismic Events Based on a Poisson Distribution

υ = Mean Annual Frequency of Exceedance
y = Number of events
t = 10,000 years

	Mean Annual Frequency of Exceedance							
	1.0E-04	5.0E-05	1.0E-05	5.0E-06	1.5E-06	1.0E-06	5.0E-07	1.0E-07
P(y = 0)	0.36788	0.60653	0.90484	0.95123	0.98511	0.99005	0.99501	0.99900
P(y = 1)	0.36788	0.30327	0.09048	0.04756	0.01478	0.00990	0.00498	0.00100
P(y = 2)	0.18394	0.07582	0.00452	0.00119	0.00011	5.0E-05	1.2E-05	5.0E-07
P(y = 3)	0.06131	0.01264	0.00015	2.0E-05	5.5E-07	1.7E-07	2.1E-08	1.7E-10
P(y = 4)	0.01533	0.00158	3.8E-06	2.5E-07	2.1E-09	4.1E-10	2.6E-11	4.2E-14
P(y = 5)	0.00307	0.00016	7.5E-08	2.5E-09	6.2E-12	8.3E-13	2.6E-14	8.3E-18
P(y = 6)	0.00051	1.32E-05	1.3E-09	2.1E-11	1.6E-14	1.4E-15	2.2E-17	1.4E-21
P(y = 7)	7.3E-05 ◈	9.4E-07	1.8E-11	1.5E-13	3.3E-17	2.0E-18	1.5E-20	2.0E-25
P(y = 8)	9.1E-06	5.88E-08	2.2E-13	9.2E-16	6.3E-20	2.5E-21	9.6E-24	2.5E-29
P(y > 0)	0.63212	0.39347	0.09516	0.04877	0.01489	0.00995	0.00499	0.00100

◈ red color indicates that the likelihood of a given number of events for certain mean annual frequency of exceedance is less than that of the regulatory limit

Table 2 Multiple Seismic Events

For a Poisson process, the mean and variance of the number of arrivals is equal to,

$$E[N] = Var[N] = \lambda = \nu t$$

The number of arrivals is controlled by the largest MAPE considered, i.e., $\nu = 1x10^{-4}$. Then, for a regulatory period of t = 10,000 years, the expected number of events with a probability of exceedance equal or lower than 10^{-4} is 1.0. As seen in **Table 2**, it is possible to have up to six

seismic events for 10,000 years and a MAPE of 10^{-4}, within the regulatory probabilistic threshold of 1 in 10,000 chance of occurrence in 10,000 years. For a regulatory period of one million years 100 events with a MAPE of 10^{-4} would be expected .

Interarrival Times

For events occurring according to a Poisson process, the time between occurrences (interarrival time) has an exponential distribution.

$$f_T(t) = \nu e^{-\nu t}, \quad t \geq 0$$

The CDF is,

$$F_T(t) = 1 - e^{-\nu t}, t \geq 0$$

Magnitude Distribution

To obtain the magnitude of the number of events taking place at each realization, the MAPEs are discretized in events with MAPEs of 10^{-4}, 10^{-5}, 10^{-6}, 10^{-7}. Because the regulatory limit is at 10^{-8}, the last 10-fold discrete value is 10^{-7}. Furthermore, the 10^{-7} threshold would be the lower significant seismic level because seismic events below MAPE of 10^{-7} are considered to have a constant PGV. For cases in which there are several discrete events with different rates of occurrence, the probability of having seismic events with a particular mean rate of occurrence is given

$$P(N[\nu_i]) = \frac{\nu_i}{\nu_1 + \nu_2 + \ldots + \nu_i + \ldots \nu_m}$$

Therefore, given that a seismic event with a MAPE of $1x10^{-4}$ or lower occurred, the probability of the seismic event for different MAPE intervals is:

$$P(N[\nu = 10^{-4}]) = \frac{10^{-4}}{10^{-4} + 10^{-5} + 10^{-6} + 10^{-7}} = 0.9$$

$$P(N[10^{-5}]) = 0.09$$

$$P(N[10^{-6}]) = 0.009$$

$$P(N[10^{-7}]) = 0.0009$$

For the TPA code, a lognormal distribution is utilized to find the ν_i for a given realization. The distribution has to be carried out for the log of the MAPE values because there are three orders of magnitude between the lower and upper MAPE values. **Figure 24** shows the lognormal distribution proposed, which corresponds to a distribution of |ln(MAPE)| + ln(10-4), with mean of

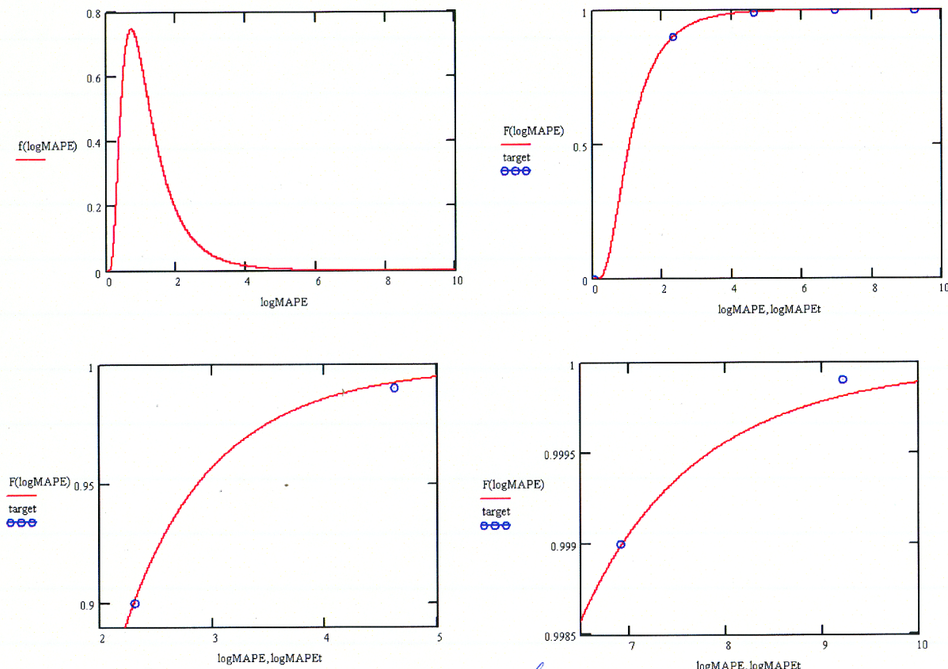

Figure 24

ln(MAPE) = 0.05, and a standard deviation of ln(MAPE) = 0.61. This lognormal distribution renders the following probability density areas for the below intervals:

- $P[MAPE < 10^{-4}] = 100\ \%$
- $P[10^{-5} < MAPE < 10^{-4}] = 90.07\ \%$
- $P[10^{-6} < MAPE < 10^{-5}] = 9.16\ \%$
- $P[10^{-7} < MAPE < 10^{-6}] = 0.67\ \%$
- $P[MAPE < 10^{-7}] = 0.08\%$

Estimation of PGV

After ν_i is known, the corresponding PGV_i is obtained by interpolating in the hazard curve of **Figure 22**.

Estimation of PGA

Because the intensity measure of the earthquake magnitude is the PGV, the PGA for a given MAPE is not unique and the corresponding dispersion has to be accounted for. The statistical PGA values for MAPEs of 10^{-5}, 10^{-6}, and 10^{-7} are presented in **Table 3**. These results are derived from fitting a lognormal distribution to the data obtained from the 15 ground motions utilized by the DOE. For intermediate MAPEs, linear interpolation is proposed to estimate the mean and dispersion. For MAPE 10^{-4} the only record provided by DOE at the emplacement level has a PGA of 0.47 g's, and a PGV of 0.47 m/s in the vertical direction. To extrapolate between MAPEs of 10^{-4} and 10^{-5}, the dispersion at MAPE 10^{-4} is assumed to be equal to that at MAPE 10^{-5}.

Table 3 Vertical PGAs for Seismic Events Associated to Different MAPEs (g)

MAPE	Mean (g)	16th (g)	50th (g)	84th (g)
$1x10^{-4}$	0.47**	-	-	-
$1x10^{-5}$	2.27	0.98	1.85	3.5
$1x10^{-6}$	4.75	2.42	4.12	7.01
$1x10^{-7}$	12.7	6.48	11.04	18.81

*** There is only one event with a target MAPE 1x10-4*

Vertical Pressures for Seismic Events

Dynamic analyses for seismic events have not been carried out to reproduce the increase on stresses in the WP OS due to DS-WP mechanical interaction. Thus, a quasi-static vertical load is used to represent the effect of potential seismic events as a function of the PGA based on the following equation:

$$P_{v,dyn} = (1 + PGA_i) P_{v,stat} F_{dyn}$$

The report "Drift Degradation Analysis" from DOE indicates that the amplification of the pressure due to seismic events is close to the mean value of the PGA. Therefore, the dynamic amplification factor, F_{dyn}, has a unit value until more refined analyses are carried out.

Compaction of Rubble after Seismic Events

The rubble accumulated around the DS is initially loosely compacted after drift degradation. The material, however, will compact with time and with shaking due to seismic events. The compaction will decrease the soil bulking factor, increasing the vertical pressure on top of the DS. The compaction mechanism, however, is not well known. The DOE has performed numerical analyses to quantify the compaction of the rubble after seismic events of different magnitude (Drift Degradation Analysis). Based on this information and compaction reported for different soil materials with time, the bulking factors will be reduced after the seismic event has finished. The reduction of the bulking factor will be proportional to the magnitude of the seismic event, see **Table 4**. Note that this effect is not important for subsequent permanent static loading because it is bounded by the shaking event that led to that compaction. In other words, if the WP did not breach under the amplification of the initial vertical pressure, it should not breach later for a compacted static load that is smaller (cumulative damage is not accounted for).

LL (03-10-06)

Table 5. Soil Compaction Range after a Seismic Event Occurs

MAPE	Compaction Factor, CF (%)
$1x10^{-4}$	10-20
$1x10^{-5}$	20-40
$1x10^{-6}$	30-60
$1x10^{-7}$	40-60

03-10-06

For a seismic event with a given MAPE, the reduction in the bulking factor will be randomly selected from a uniform distribution with lower and upper values dictated by the above table. Because NRC/CNWRA staff indicated that the majority of the bulking factors are located between 1.15 and 1.25, the bulking factors should not be reduced below 1.15. For the few realizations in which the bulking factor is already smaller than 1.15, no further reduction is performed. Note that the bulking factor reduction is based on the expansion of the rock volume (the fraction exceeding the unit).

The rationale developed in previous pages is used to developed the following static and dynamic loading algorithms.

Algorithm for DS Collapse and DS-WP Interaction under Static Loading

This section includes a summary of the steps required to evaluate DS collapse and static DS-WP interaction in MECHFAIL.

*** Drip Shield Performance**

* Select the bulking factor from a standard beta distribution [0,1]+1, $\mu_{BF} = 0.2$, $\sigma_{BF} = 0.037$

* Randomly select the carving failure mechanism for the drift with a weighted average of 0.75 for piping mechanism, and 0.25 for Terzhagi mechanism

* Obtain the demand vertical pressure on top of the DS from the relationship between the bulking factor value and the failure mechanism (**Figure 14**).

* Select the drift degradation time based on a lognormal distribution with median $\hat{t} = 750 yrs$, and $\sigma_{\ln t} = 0.23$

* Obtain the temperature of the DS and WP using as one of input parameters the drift degradation time (out of MECHFAIL module)

* Randomly select the horizontal to vertical load ratio for the DS using a standard beta distribution [0,1], $\mu_{Ph/Pv} = 0.5$, $\sigma_{Ph/Pv} = 0.11$

* Use the horizontal to vertical load ratio to obtain the DS vertical load carrying capacity ($P_{v,DScap}$) using the polynomial and logarithmic equations of **Figure 17b**. Also, compute the DS capacity at the initiation of yielding as

$$P_{v,DSyield} = P_{v,DSyield} * C_{yield}$$

where C_{yield} is a constant. A variable yielding to ultimate DS capacity ratio was originally suggested, but the C_{yield} constant was adopted because the yielding capacity is very close to half of the ultimate capacity for most of the evaluated loading configurations. Then, C_{yield} = 0.5

* Modify the DS vertical load carrying capacity, and the DS capacity at yielding, by the temperature multiplier:

$$P_{v,DScap} = P_{v,DScap} * F_{temp}$$

03-10-06

$$P_{v,DSyield} = P_{v,DSyield} * F_{temp}$$

where the multiplier is obtained by linearly interpolating from the following data:

F_{temp} = 1.0 for $T \leq$ 150 degrees Celsius
F_{temp} = 0.78 for T = 260 degrees Celsius
F_{temp} = 0.64 for $T \geq$ 316 degrees Celsius

* Modify the DS vertical load carrying capacity obtained in the previous step by applying the creeping multiplier:

$$P_{v,DScap} = P_{v,DScap} * F_{creep}$$

The creeping multiplier is the combination of two factors. The first one reduces the DS vertical load carrying capacity to the DS yielding capacity using the yielding constant, C_{yield}, described above. The second factor randomly selects the creeping threshold (with respect to the yielding stress) for creeping failure from a uniform distribution. Then,

$$F_{creep} = C_{yield} * rand[0.9,1.2]$$

* Modify the DS vertical load carrying capacity, and the DS yielding capacity, obtained in the previous step by applying the DS corrosion multiplier:

$$P_{v,DScap} = P_{v,DScap} * F_{DS,t}$$

$$P_{v,DSyield} = P_{v,DSyield} * F_{DS,t}$$

The DS corrosion multiplier is function of the DS corrosion rate obtained out of MECHFAIL, assuming that the DS plate is 15 mm thick (as the shell plate). Then, the factor is is divided into two parts:

For thickness plates after corrosion between $t_{p,i}$ = 0 and 7.5 mm, $F_{DS,t} = 0$

For thickness plates after corrosion between $t_{p,i}$ = 7.5 and 15 mm,

$$F_{DS,t} = 0.25 + 0.1(t_{p,i} - 7.5)$$

* Compare demand vertical pressure to DS vertical load carrying capacity

If $P_{v,dem} > P_{v,DScap}$ then
The DS collapses and DS - WP mechanical interaction is evaluated
Indicate that the DS collapses due to static loading

03-10-06

If $P_{v,dem} > P_{v,DScap}$ then
If seismic event with MAPE $\leq 1x10^{-5}$ occurs the DS collapses
If seismic event with $1x10^{-5}$ < MAPE $\leq 1x10^{-4}$ occurs then
If (static stresses, $P_{v,dem}$ > yield stresses, $P_{v,DSyield}$) then
DS collapses
else
check seismic algorithm
endif
endif

****** DS - WP Mechanical Interaction**

* Select contact angle for the interaction based on a normal distribution with mean $\mu_\alpha = 0$, and standard deviation, $\sigma_\alpha = 10$.

* Obtain the force per unit length (F_{unit}) based on the polynomial equation of **Figure 19** (Figure 19 was modified.)

* The contact length (L_{cont}) of the DS component is obtained from a normal distribution with mean $\mu_{Lcont} = 500mm$, $\sigma_{Lcont} = 100mm$

* The WP OS vertical load carrying capacity is derived from the following equation:

$$P_{v,WPcap} = \frac{F_{unit}}{A_{trib}} \frac{L_{cont}}{L_{unit}}$$

where A_{trib} is the tributary area to the DS bulkhead. To obtain the tributary area is considered that the bulkheads are spaced at each 1.047 m, and that in case of complete failure of the DS columns (support beams), the width of the tributary area would be about 2.0 - 2.5 m. Therefore, the tributary area is set as A_{trib} = 2.3 m^2. On the other hand, the adimensional term L_{cont} / L_{unit} has as numerator the contact length, whereas the denominator is the unity.

* Compare demand vertical pressure to DS vertical load carrying capacity

If $P_{v,dem} > P_{v,WPcap}$ then
Indicate that the WP fails due to static loading

If $P_{v,dem} < P_{v,WPcap}$ then
Indicate that the WP does not fail due to static loading
Go to the dynamic loading algorithm

03-10-06

Summary of Seismic Events Abstraction in MECHFAIL

The following steps summarize the seismic abstraction. The steps are presented in a series of logic steps using commands included in most programming languages, but the algorithm is not a substitute for the codification to be carried out by the performance assessment staff.

t_i = time of each seismic event
T = postclosure period
T_{DScorr} = time at which the DS corrodes completely
T_{seism} = period for computing seismic events

$i = 0$
$t_i = 0$
$v_{\min} = 1x10^{-4}$
$BF_0 = BF$, BF is the bulking factor computed originally

estimate T_{DScorr} (out of MECHFAIL)
select time for evaluating seismic events: $T_{seism} = \min(T, T_{DScorr})$

while $t_i < T_{seism}$
$i = i + 1$

***** Obtain the time for the next seismic event

$F_T(t) = rand()$, $0 \le rand() \le 1$
$t = -\ln[1 - F_T(t)] / v_{\max}$,
$t_i = t_i + t$
$if\,(t_i > T) end\_while\_loop$

***** Obtain the mean rate of recurrence,

$dummy = rand()$, $0 \le rand() \le 1$

... use the random value to obtain v_i based on the lognormal CDF of the log of the MAPE values.

***** Obtain the peak ground velocity

$PGV_4 = 0.47$, *PGV* at 1x10^{-4} (m/s)
$PGV_5 = 1.07$

03-12-06

$PGV_6 = 2.44$
$PGV_7 = 5.35$
$PGV_{<7} = 5.35$

... Interpolate based on the above PGV data to obtain PGV_i for v_i

***** Obtain mean and standard deviation of the log of the data for *PGA (use mean instead of median values, Ron already did this)*

$mean_{PGA,4} = 0.47$, $stdev_{PGA,4} = 0.64$
$mean_{PGA,5} = 2.27$, $stdev_{PGA,5} = 0.64$
$mean_{PGA,6} = 4.75$, $stdev_{PGA,6} = 0.53$
$mean_{PGA,\le 7} = 12.70$, $stdev_{PGA,\le 7} = 0.53$

... interpolate to obtain the PGA mean and standard deviation, $mean_{PGA,i}$ and $stdev_{PGA,i}$

... use the computed PGA parameters of a lognormal distribution to create the corresponding CDF

... use a random value to obtain PGA_i from the lognormal CDF of last step

***** Obtain the time - Alloy-22 plate thickness relationship (out of MECHFAIL). Compute the updated $P_{v,stat}$ according to the Alloy-22 plate thickness reduction with time, and the thickness plate multiplier of Figure 21

$P_{v,stat} = P_{v,stat} * F_{tp}$

***** Use the obtained PGA_i to approximate the increase on the vertical pressure during the seismic event

$F_{dyn} = 1$, dynamic amplification factor
$P_{v,dyn} = (1 + PGA_i) P_{v,stat} F_{dyn}$

03-12-06

***** If the DS has not failed due to static loading compare the dynamic demand vertical pressure to the DS capacity. Otherwise, verify the WP performance

If (DS has not failed due to static loading or previous seismic events) then

If $P_{v,dyn} > P_{v,DScap}$ then

Indicate that the DS fails due to dynamic loading

If $P_{v,dyn} < P_{v,DScap}$ then

Indicate that the DS does not fail due to the current seismic event

endif

if (DS has failed due to static loading or any seismic event)

If $P_{v,dyn} > P_{v,WPcap}$ then

The WP fails due to dynamic loading

If $P_{v,dyn} < P_{v,WPcap}$ then

Indicate that the WP does not fail due to the current seismic event

endif

***** Compute the bulking factor after shaking

$$if\,(1x10^{-5} < v_i \le 1x10^{-4})then$$

$$CF_i = 0.10 + rand()[0.20 - 0.10],$$ *rand()* = random value between [0,1]

$$elseif\,(1x10^{-6} < v_i \le 1x10^{-5})then$$

$$CF_i = 0.20 + rand()[0.40 - 0.20]$$

$$elseif\,(1x10^{-7} < v_i \le 1x10^{-6})then$$

$$CF_i = 0.30 + rand()[0.60 - 0.30]$$

$$elseif\,(v_i \le 1x10^{-7})then$$

$$CF_i = 0.40 + rand()[0.60 - 0.40]$$

$$endif$$

$$if\,(BF_{i-1} > 1.15)then$$

$$BF_i = 1 + (BF_{i-1} - 1)(1 - CF_i)$$

$$if\,(BF_i < 1.15)then$$

$$BF_i = 1.15$$

$$else$$

$$BF_i = BF_{i-1}$$

$$endif$$

03-10-06

... Compute $P_{v,stat}$ for the new bulking factor BF_i. The updated vertical pressure will be used in the next seismic event

03-10-06

$$endwhile$$

WP FAILURE MODE

Under NRC request, the BNL-2 staff developed a write-up to ~~define~~ describe the current failure mode of the first stage of numerical analyses, and to plan the improvement in the numerical models for the second stage. LI (03-13-06)

A discussion about engineering and true stress-strain relationships is also included.

Luis Ibarra

From: Luis Ibarra [libarra@cnwra.swri.edu]
Sent: Friday, February 17, 2006 5:47 PM
To: 'Mysore Nataraja'
Cc: 'bsagar@cnwra.swri.edu'; 'ACHOWDHURY.CNWRA.Internet@nrc.gov'; 'smohanty@cnwra.swri.edu'; 'Mahendra Shah'; 'Aladar Csontos'; 'Thomas Wilt'; 'ofoegbu@cnwra.swri.edu'
Subject: Failure mode and true stresses

Raj,

As we discussed this week, I am attaching a write up with the assumptions and the reasons for selecting the WP failure mode that is described in the draft of the DS-WP interaction analysis. Also, I am including some points about the true and engineering stress – strain relationships.

Feel free to distribute to the people you consider appropriate, and let us know when you want to have a meeting on this issue.

Thanks.

Luis

03-13-06

WP Analytical Failure Mode for First Stage of FEMs in MECHFAIL

The waste package outer shell (WP) may be subjected to concentrated stresses due to static and dynamic loads transferred by the drip shield (DS) components. The WP is composed of two rings. The WP "outer shell" (OS) is the external ring, a 20 mm-thick plate of Alloy-22. The internal ring is a 50 mm-thick plate of stainless steel named "inner vessel." Failure of the WP is associated to breaching of the WP OS and the WP inner vessel, resulting in cracks or holes that propagate throughout the entire plate depth. An assessment of this nature involves complex numerical analyses and a lot of interaction between ENG-2 group and other disciplines. Therefore, the study was divided into two stages, and several assumptions that simplify the computations and expedite the time for obtaining the mechanical abstractions were implemented. Time is an important factor because ENG-2 group has the responsibility of providing the mechanical abstractions to the performance assessment (PA) group in a reasonable time frame. To perform the WP evaluation, the following assumptions were adopted:

1. WP failure occurs when the WP OS breaches because the inner vessel is made of stainless steel, a material with very high deterioration rate when exposed to Yucca Mountain environmental conditions. Therefore, the function of the inner vessel is limited to provide structural support to the WP OS.

2. Stress corrosion cracking (SCC) is highly unlikely in Alloy-22 at YM. This assumption is based on work developed by the DOE and CNWRA staff (He and Dunn, 2006), which indicates that the environmental and electrochemical conditions for developing SCC are very unlikely at the emplacement level at YM. The evaluation of SCC is performed under high stress levels. However, it must be noted that CNWRA staff still has to verify that SCC is unlikely for a state of stresses that reaches, or even surpasses, the ultimate tensile strength (UTS).

3. Localized corrosion does not affect mechanical stresses. CNWRA staff conducted several tests to evaluate crevice corrosion propagation in the WP OS material (Shukla et al, 2006). Although crevice corrosion of Alloy 22 is possible under some conditions, the maximum penetration depth of localized attack may be limited to depths significantly less than the container thickness as a result of stifling and repassivation of crevice corrosion.

4. Uniform corrosion is partially coupled to mechanical stresses. Generalized corrosion rates are very small and are not significant for the initial regulatory period of 10,000 years. However, the compliance period was extended to a million years and generalized corrosion may cause significant thinning of the WP plates during this extended period. To include this effect, the numerical evaluations are performed for several plate thicknesses, and a relationship between WP capacity and plate thickness is obtained.

03-13-06

5. A continuum finite element model (FEM) is proposed. This assumption is reasonable because

Alloy-22 is a highly ductile material that usually exhibits large deformations without cracking. In addition, experimental tests indicate that SCC and localized corrosion are highly unlikely due to the environmental and electrochemical conditions at YM.

6. Physical failure of the WP OS occurs at the fracture strain. Figure 1 presents the engineering stress - strain curve for a tensile test of Alloy-22 material. After the peak strength of the engineering stress-strain curve, necking of the material initiates, stress distribution is not uniform, and a large reduction in area occurs. This item assumes that the WP OS does not present cracks until fracture strain occurs, implying that Alloy-22 will not exhibiting cracks, even if necking of the material occurs. Experimental data still is needed to validate this assumption.

7. In a first stage, the analytical WP OS failure mode is associated to the first element reaching the strain of the UTS. It has to be clear that this failure definition does not predict breaching of the WP OS, and simply finds a potential onset for WP breaching. This is an accepted definition for collapse used in several structural guidelines (e.g. FEMA 356, 2000) because of the large uncertainties and complexities involved in obtaining and modeling deteriorating constitutive relationships. Below are discussed the numerical analyses that can be developed to overcome the limitations of this failure definition.

The ENG-2 staff held several meetings from October to December of 2005 to discuss the path forward to provide reasonable mechanical abstractions in a short time frame to the PA group. Based on these discussions, the definition of failure mode for the first stage of FEA was sent to NRC staff on December 16, 2005. The FEMs developed for this stage include non-deteriorating models that reproduce the structural performance until the UTS is reached. The FEMs require deteriorating constitutive relationships expressed in terms of true stresses and strains until the UTS. These values can be obtained from engineering stress - strain relationships using analytical closed form solutions that assume uniform deformation.

If the physical failure mode of assumption (6) is accurate, the analytical failure mode is conservative for the following reasons:

a) Failure mode is based on the UTS. Once the UTS is surpassed, a system with no redundancy is structurally unstable under monotonic loads. In the case of the WP OS, however, the system should be able to redistribute some of the stresses and increase its loading capacity. This increase in capacity is expected to be marginal because the material has already increased significantly its resistance into the nonlinear range, and because the strain at the UTS is close to the ultimate strain. In addition, the softening of the engineering stress-strain curve after the UTS exhibits a steep negative slope, indicating that the loss of resistance takes place rapidly (Figure 1.) That is to say, Alloy-22 material can be considered a brittle material after the UTS is surpassed.

03-13-06

b) Failure is assumed as soon as the first Alloy-22 element reaches the UTS. This

assumption is necessary because ABAQUS/Standard cannot remove from the calculations elements that have failed. This is a common assumption, which has also been adopted in the DOE evaluations. It is difficult to predict the level of conservatism induced by this decision. On one hand, it is possible that as the DS component penetrates into the OS, the contact area increases and arrests the breaching of the WP. However, it may happen that failure of the first elements propagates and leads to a band of damaged elements with no strength resistance, which cannot be deterred even if the contact area increases.

c) The DS components may reach the UTS previous to analytical failure of the Alloy-22 material. Because non-deteriorating models do not lose resistance capacity, the DS component resistance is overestimated, which leads to smaller contact areas than those expected in the physical models.

d) The stress - strain curve in ABAQUS is approximated by a bilinear relationship that corresponds to the lower boundary for stresses between the already defined yielding and UTS points.

On the other hand, even with the conservatism introduced by the definition of the analytical failure mode, the analyses still are much closer to the real performance than the current MECHFAL abstraction. The following are some of the reasons leading to this conclusion:

i) The DS component can exhibit linear and nonlinear deformations, increasing the contact area between the DS and the WP

ii) The reaching of the UTS of Alloy-22 is considered the failure stress level, a very high stress level when compared to most of the traditional numerical analyses

iii) The mechanical material properties are not obtained from standards or conservative assumptions. The properties are based on comprehensive experimental data that consider the effect of different temperature, strain rates, and direction of the load, on the mechanical properties of Alloy-22

iv) The analytical failure mode assumes that cracks do not propagate until the UTS is reached

v) Different loading scenarios are included in a sensitivity study, such as different contact angles and boundary conditions.

03-13-06

8. The analytical failure mode is based on the WP capacity. Failure of the system is based on the vertical load carrying capacity that the WP can withstand, instead of displacements or ductilities values at failure. The disadvantage of the approach is that the failure mode is not directly linked to the potential breaching of the WP OS, particularly because non-deteriorating constitutive

relationships are used. The advantage of this methodology is that as failure is approached, the capacity of the system increases marginally whereas parameters such as displacements become very unstable at this stage. Therefore, the definition of failure as a function of the system capacity is more reliable.

9. More advanced FEMs may be required in the second stage of the study. There are two main reasons for developing more complex numerical analyses: i) the analytical failure of the FEMs in the first stage is not associated to breaching of the WP OS, although predicts an onset of collapse that may be very close to breaching in terms of capacity, and ii) seismic loading is not evaluated in the first stage in a comprehensive manner.

The most likely model to be used in the second stage is a continuum damage mechanics model. The model should be capable of accounting for the softening/damage region of the of the engineering stress-strain curve. The "crack" in the material would be represented by the resulting bands of damaged elements which have no stiffness associated with them. Mesh dependence (characteristic lengths of the elements) of the solutions will need to be addressed.

In ABAQUS, the classical metal plasticity models can be used in conjunction with the models of progressive damage and failure in ABAQUS/Explicit to specify different damage initiation criteria to account for progressive degradation of the material stiffness and the removal of elements from the mesh. By using this approach, material failure refers to the complete loss of load carrying capacity that results from progressive degradation of the material stiffness. The stiffness degradation process is modeled using damage mechanics.

In ABAQUS/Explicit, the degradation of the model is based on the engineering stress - strain curve. The program recognizes that a marked reduction of the load carrying capacity takes place beyond the peak strength until rupture. The deformation during this last phase is localized in a neck region of the specimen. In ABAQUS, the peak strength of the engineering stress- strain curve is referred as the damage initiation criterion. Beyond this point, the stress-strain response is governed by the evolution of the degradation of the stiffness (and strength) in the region of strain localization. Therefore, the damage evolution law has to be provided based on the engineering stress-strain curve, and cannot be obtained by feeding the model with the true stress - strain curve beyond necking initiation in ABAQUS/Standard.

This assumption requires experimental results indicating that cracks do not occur previous to the rupture strain. If significant cracks occurred previous to fracture of the material, the above deteriorating model still would be applicable, but the definition of failure would have to be modified.

03-13-06

Another option that has been analyzed is the use of fracture mechanics analyses. These FEMs would use a two-surface, double node in the zone in which the crack is assumed to occur. In this approach, a zone containing master and slave surfaces is created. The surfaces are initially in

contact (i.e. bonded together). The propagation of the crack through the material would be simulated using a "debonding" criterion, which may use normal and shear components. In any case, the continuum deteriorating model is favored over this fracture analysis.

In summary, the analytical failure mode for the first stage of the DS - WP interaction evaluation considers assumptions that simplify the numerical evaluation and are consistent with the available information that can be used in a performance assessment. The failure mode definition is also acceptable because the FE results indicate that there is a large safety margin against breaching of the WP OS due to static loads, and possibly, adequate performance under dynamic loading. The second stage of the study includes deteriorating FEMs that have to be carried out on ABAQUS/Explicit. These models will be able to account for the softening of Alloy-22 material after the peak strength, and will be used to evaluate dynamic loading due to seismic events. In the meantime, experimental tests have to be carried out to obtain the performance of the WP material when subjected to highly nonlinear stresses.

Discussion on Engineering versus True Stress - Strain Curves

The true stress - strain curves present more realistic information of the stresses in the material because are based on the deformed shape of the specimen. For this reason, plastic analyses require the input of uniaxial true stresses and strains when larger deformations can occur. All FEMs developed for the DS - WP interaction include true stresses and strains.

Analytical solutions exist to obtain true stresses until the peak strength is reached because the deformation is uniform and engineering stress - strain relationships can be used. However, the uniform extension ceases when the tensile load reaches the UTS. At this point, the test samples begin to neck, and the state of stresses changes gradually from the simple uniaxial tension to a complicated condition of triaxial stresses. It is not possible to determine a uniaxial true stress-strain relation by the standard tensile test once necking has started because once deformation is not uniform, only averages stresses can measured and the stress distribution cannot be determined (Ling, 1996). This is the main reason for the problems encountered to obtain the true stress after necking. Furthermore, empirical relationships to obtain true stress-strain curves depend on the sample geometric characteristics because the uniaxial state of stresses does not apply after necking.

An important observation during the necking stage is that the true stresses increase significantly, mainly because of the reduction in area. However, the capacity of the system does not increase, as deducted from the reduction in the applied force after the UTS is surpassed. Therefore, true stresses in the necking stage are not necessarily translated into a large increase in the overall capacity of the system. Moreover, as discussed above, the proposed deteriorating models for the

03-13-06

second stage of FEMs do not require true stresses after necking, but a damage evolution law that can be obtained directly from the engineering stress - strain curve.

REFERENCES

FEMA 356 (2000), "Prestandard and commentary for the seismic rehabilitation of buildings," *Federal Emergency Management Agency*, Washington D.C.

He, H, and Dunn, D.S. (2006) "Crevice Corrosion Penetration Rates of Alloy 22 in Chloride-Containing Waters", Paper 06618, Symposium: Nuclear System Corrosion (06-TEG-224X)

Ling, Y. (1996) "Uniaxial True Stress-Strain after Necking," *AMP Journal of Technology*, Vo. 5, June 1996

Shukla, P.K., Dunn, D.S., Chiang, K.-T., and Pensado, O. (2006) "Stress Corrosion Cracking Model for Alloy 22 in the Potential Yucca Mountain Repository Environment", Paper 06502, Symposium: Environmentally Assisted Cracking (06-TEG-186X)

FIGURES

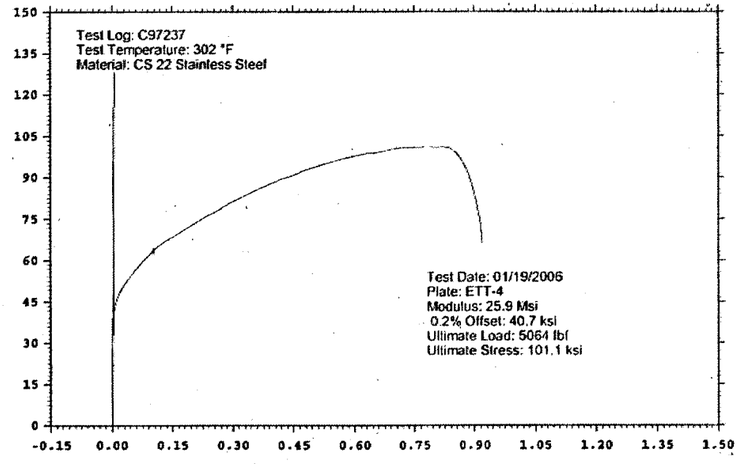

Figure 1 Engineering Stress - Strain Curve for Alloy-22 Material at 150 C

03-13-06

APPENDIX

Derivation of True Stress - Strain Relationship from Engineering Stress - Strain Curve

This appendix presents an example for obtaining the true stress - strain curve from the engineering stress - strain relation. The data for the latter curve corresponds to Alloy-22 tensile tests subcontracted by CNWRA to Westmoreland labs (see Figure 1). The below derivation obtains the true UTS and fracture points. The true UTS is obtained from an analytical closed form solution that assumes uniform distribution until the reaching of the UTS. The information for the UTS is the same used in the ABAQUS models of the first stage. The true fracture stress and strain is based on simplifications and empirical equations, and corresponds to the lower boundary for the true stresses. It is emphasized that the large true stresses in the neck region (after the UTS) take place under decreasing applied loads.

The engineering ultimate tensile strength (UTS) is s_{UTS} = 697 Mpa (100.1 Ksi), whereas the strain at the UTS is about $e_{UTS} = 0.75$. Assuming that until the UTS the deformed volume of the sample is conserved, the true stress and strain previous to UTS can be computed as:

$$\sigma = s(1+e),\ \varepsilon = \ln(1+e) \qquad (1)$$

For the above case,

$$\sigma_{UTS} = 697 * (1+0.75) = 1220\,MPa$$

The corresponding true strain would be,

$$\varepsilon_{UTS} = \ln(1+0.75) = 0.56$$

The reduction in area at fracture is,

$$R_{area} = \frac{A_o - A_{frac}}{A_o} = 0.765$$

Also, the area at fracture, A_{frac}, can be expressed as,

$$A_{frac} = A_o(1 - R_{area}) \qquad (2)$$

Then, the true fracture strain is based on the original area and the area after fracture. Equation

03-13-06

(1) is not valid beyond the onset of necking, it is not possible to calculate the true fracture strain from measure values:

$$\varepsilon_{frac} = \ln\frac{A_o}{A_{frac}}$$

After substituting the fractured area using Equation (2), the true fracture strain for cylindrical tensile specimens is expressed as

$$\varepsilon_{frac} = \ln\frac{1}{1 - R_{area}}$$

The true strain at fracture is $\varepsilon_{frac} = 1.46$

True stress at fracture

The load at fracture can be obtained from the engineering stress, which is based on the initial area of the specimen,

$$s = \frac{P}{A_o}$$

Then, at the applied force at fracture is,

$$P_{frac} = s_{frac} A_o$$

$$P_{frac} = 482e^6\,Pa(3.233e^{-5}m^2) = 15584N = 15.58KN$$

The applied load at fracture is less than the maximum applied load of 22560 KN at the UTS.

The true fracture stress is the load at fracture divided by the cross-section area at fracture.

$$\sigma_{frac} = \frac{P_{frac}}{A_{frac}} = \frac{P_{frac}}{A_o(1 - R_{area})}$$

03-13-06

$$\sigma_{frac} = \frac{15584N}{3.233e^{-5}m^2(1-0.765)} = 2051MPa$$

The above fracture stress should be corrected for the triaxial state of stress existing in the tensile specimen at fracture. This information is often not available, and true fracture stress values are frequently in error.

It has been suggested that the curve of many metals in the region of uniform plastic deformation can be expressed by a power curve relation.

$$\sigma = K\varepsilon^n$$

where n is the strain hardening exponent and K is the strength coefficient. It can be proved (Nasser et al, 1999) that at necking, the true uniform elongation is equal to the strain hardening exponent.

$$n = \varepsilon_{UTS}$$

For the above case, $n = 0.56$.

The strength coefficient must be equal to $K = 1688.08$ in order to obtain the true stress at the UTS. Ling (1996) suggests that the power law may be useful for extrapolation of the true stress-strain curve beyond necking. Actually, Ling (1996) indicates that the power law appears to underestimate true stresses and the extrapolation provides a lower bound for the true stresses. By extrapolating the power equation until the above computed fracture strain, it is obtained that σ_{frac} = 2086 Mpa, which is close to the value obtained using the fractured area and the applied load at fracture.

03-13-06

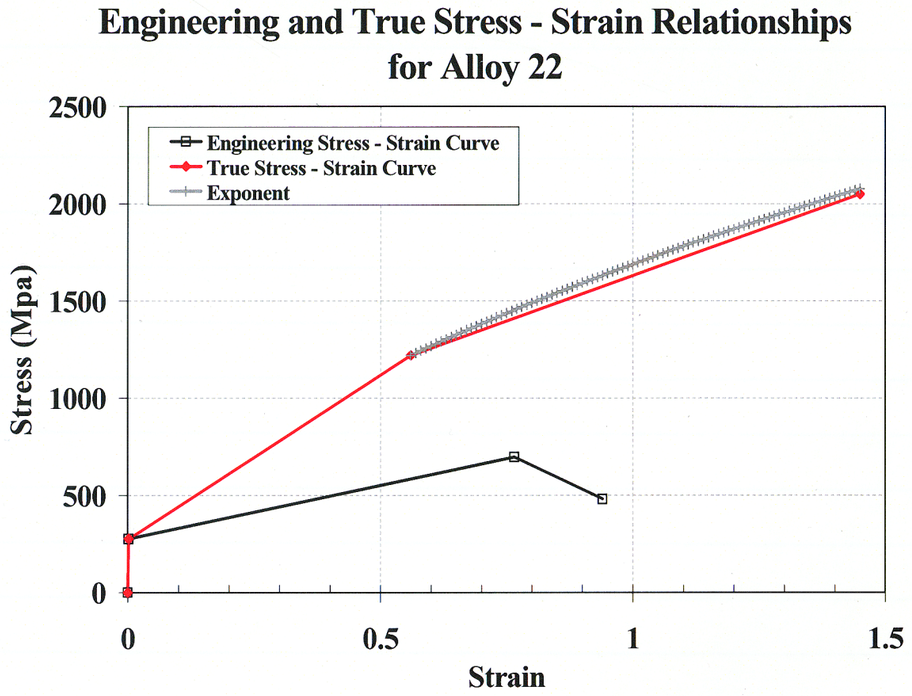

Figure A1. True and Engineering Stress - Strain Curves

03-13-06

GEOSCIENCES AND ENGINEERING DIVISION

SCIENTIFIC NOTEBOOK REVIEW CHECKLIST RECORD

Scientific Notebook No. 656 Project Numbers: 20.06002.01.342

Accomplished

- [x] 1. Initial entries per QAP-001
- [x] 2. Dating of entries
- [x] 3. Corrections (crossed out, one line through w/initials/date)
- [x] 4. No White out used
- [x] 5. Page number visible on copy or original notebook
- [x] 6. In process entries per QAP-001
- [x] 7. Figure information present
- [x] 8. Text readable
- [x] 9. Copyrighted material is identified
- [x] 10. Permanent ink or type only
- [x] 11. Signing of entries (not required on each page)
- [x] 12. Electronic media in the scientific notebook properly labeled
- [x] 13. NRC Supplementary Scientific Notebook Questions are addressed.
- [x] 14. The independent, two person verification required by AP-019, Section 5.2.1.2(b) is complete

Any discrepancies must be resolved before notebook closeout.

==========

I have reviewed this scientific notebook and find it in agreement with QAP-001.

Manager's Signature 9-27-2007 Date

Attach this completed form to the last page of the notebook.